ACS Macro Letters

Letter

pubs.acs.org/macroletters

Submicrometer 3D Structural Evidence of Fuel Cell Membrane Heterogeneous Degradation

Marco Maccarini,[†,‡] Sandrine Lyonnard,[‡] Arnaud Morin,[*,§] Jean Francois Blachot,[§] Emanuela Di Cola,[∥] Govind Prajapati,[‡] Michael Reynolds,[∥] and Gérard Gebel[§]

[‡]University Grenoble Alpes, INAC-SPrAM, CEA, INAC-SPrAM, and CNRS, SPrAM, F-38000 Grenoble, France

[§]University Grenoble Alpes, F-38000, and CEA, LITEN, 17 rue des Martyrs, 38054 Grenoble Cedex 9, France

[∥]ESRF, 71 rue des Martyrs, CS 40220, 38043 Grenoble Cedex 9, France

Supporting Information

ABSTRACT: Polymer membranes used in the proton exchange membrane fuel cell (PEMFC) technology are subject to severe chemical and physical degradations during operation. A microscopic diagnosis of the effects of aging on the microstructure of benchmark perfluorinated sulfonic acid (PFSA) membranes is crucial to developing long-lasting devices. We report here the first μSAXS study of membranes aged for 2500 h in a stack. SAXS spectra recorded with submicrometer resolution in-plane and along the membrane thickness provide a 3D mapping of the aging effect. Nanoscale heterogeneities are evidenced and found to depend on the membrane position relative to the electrodes, to the air inlets, and proximity to channels (distributing gas) or ribs (collecting the current). Long-term aging in a fuel cell operating in stationary conditions around 65 °C results in a small voltage degradation rate of 13 μV/h, without any evidence of membrane failure, but to an irreversible over-swelling of the membrane due to polymer relaxation. Regions under the gas distribution channels close to the air inlet are profoundly degraded due to an increased water gradient concentration from the cathode to the anode. These observations provide a novel and unique insight for developing new strategies toward the design of more durable polymers inserted in smart fuel cells.

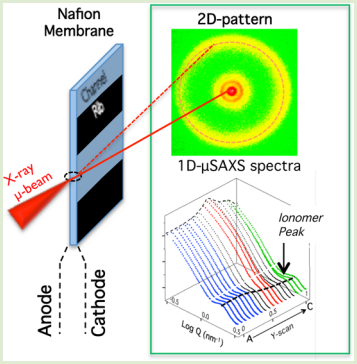

The limited lifetime of proton exchange membranes hinders the development of next generation electrochemical devices for energy storage and conversion. With the objective of clean fossil-free automotive and stationary applications, long-lasting high performance proton exchange membrane fuel cells (PEMFC) are required. The PEMFC technology is based on polymer membranes acting as proton conducting electrolyte and electrode support. The design of durable PEM is a prerequisite for large-scale commercialization of electrochemical energy storage devices. The degradation of the membrane produces a continuous drop in performance during operation, leading to a detrimental dysfunction and ultimately fuel cell failure. This technological and industrial challenge has drawn considerable attention to fundamental research, stimulating a number of experimental studies dedicated to unraveling the effects of aging.[1−3] However, the microscopic origin of the various chemical, electrochemical, and physical degradation mechanisms in play is mostly unknown, even in state-of-the art benchmark perfluorinated sulfonic acid (PFSA) materials.

From a physical viewpoint, scanning and transmission electron microscopy studies showed that aging depends on the fuel cell operating mode (on−off or freeze−thaw cycling) and local conditions (temperature, humidity, current density).[4] Each single cell of a PEMFC stack is composed of a membrane assembled with platinum−carbon electrodes and gas diffusion layers. This membrane-electrodes assembly (MEA) is sandwiched between bipolar plates serving as current collectors (via ribs) and gas distributors (via channels). A severe mechanical fatigue of the membrane results from swelling cycles in such a constrained environment.[5,6] Cracks, holes, and local delamination have been observed.[7,8] Highly heterogeneously degraded zones were also evidenced on aged membranes, both in-plane and along the thickness, depending on the membrane position relative to gas inlets, ribs, or channels.[9] These findings brought insight into the macroscopic effects, yet calling for a deeper understanding down to the microscopic level. From a chemical viewpoint, polymer degradation was probed via the release of fluorine and sulfonated species in the water produced by the fuel cell[10,11] and in-depth profiling of aged Nafion cross sections by microFTIR.[12] However, the impact of long-term operation on membrane microstructure has not been addressed to date, although proton transfer efficiency and PEMFC performances are largely governed by the morphology of the hydrated nanophase-separated polymer. Since the 80s, small-angle and wide-angle X-ray scattering techniques (SAXS/WAXS) were extensively used to study ion-containing nano-separated membrane microstructures.[13] More recently, new opportunities stemmed from the availability of intense,

Received: March 27, 2014
Accepted: July 11, 2014
Published: July 24, 2014

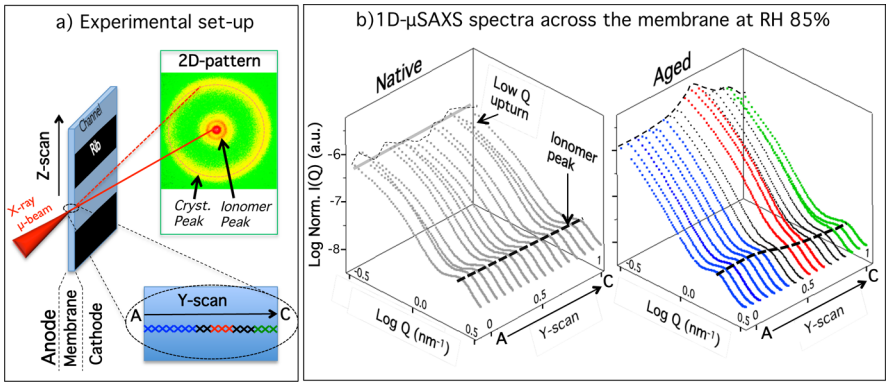

Figure 1. (a) Schematic view of the experimental setup. The microfocused X-ray beam is directed onto the membrane at various vertical z-positions. 2D diffraction patterns are recorded during horizontal y-scans along the membrane, from the anode (A) to the cathode (C) side. (b) Radially averaged 1D spectra $I(q)$ vs q, obtained in native membrane (left) and in a section of MEAs close to the air inlet and in front of the channel (right). y-Scan spectra series recorded at 85%RH show, respectively, the homogeneous (native) and heterogeneous (aged) microstructure along membrane thickness.

micrometer-sized X-ray beams produced by the world-class high brilliance synchrotron sources. The micro-SAXS (μSAXS) technique was released as a unique means to obtain spatially resolved 3D mappings of complex nanostructures. It has been successfully employed to evidence the anisotropic structure of sulfonated polyimide membranes[14] and ice crystal formation on membrane surfaces stored at low temperature.[15,16] Herein, we show that μSAXS can bring invaluable information on structural heterogeneities induced by long-term aging. We report the first 3D submicrometer investigation of the structural evolution of PFSA membranes integrated in a PEMFC stack aged for 2500 h at 65 °C in counter-flow configuration. The current density was fixed at 0.5 A/cm^2, and gas pressures and inlet relative humidity (RH) being equal to 1.5 bar and 75%, respectively. Such operational conditions lead to an average degradation rate of the voltage of each cell as low as 13 μV/h without any significant increase of H_2 crossover or any evidence of membrane failure. The operating conditions were representative for stationary applications, that is, much softer than open circuit voltage tests. Various zones of aged membranes were studied: close to or far from gas inlet, under ribs or under channels, and anode- or cathode-sided. As aging translates into clear signatures on the scattering μSAXS profiles, we are able to build a comprehensive picture of membrane heterogeneous degradation with unprecedented spatial resolution in-plane and along the membrane thickness. The result of this work is a detailed diagnosis of micro-to-macro correlations through the quantitative inspection of polymer morphology degradation as a function of cell design parameters and local operating conditions.

The μ-SAXS experiment was carried out at the European Synchrotron Radiation Facility (ESRF, Grenoble, France) on the microfocus ID13 beamline. Aged MEAs (2500 h) from SolviCore under the reference R400, which is made up of 50 μm thick short side chain nonreinforced PFSA membranes, were investigated. Pieces of the aged MEAs were cut either close or far from the air inlet (more details on MEA samples and preparation are given in the Supporting Information, Figure S1). They will be referred to as "inlet" and "middle" positions in the text. A fresh membrane was also measured as a reference. The various samples were mounted on a dedicated cell, allowing relative humidity control, and positioned at the beam focal spot (Figure S1).[17] A sketch of the experimental setup is shown in Figure 1a (see Figure S2 for more details). The instrument was configured to work in a momentum transfer Q (defined as $4\pi\cdot\sin(\theta)/\lambda$, where θ is the scattering angle) spanning from 0.3 up to 30 nm^{-1}. Different vertical positions (z-axis) were chosen to select zones under ribs or channels. At a fixed z-position, the two-dimensional scattering patterns were then acquired over linear scans along the membrane thickness (y-scan) from anode to cathode side, with typically 2−5 μm step size. All native and aged membrane spectra display two characteristic isotropic features, as shown in Figure 1a: a WAXS maximum at high Q (around 12 nm^{-1}) related to the local packing of perfluorinated polymer chains in amorphous and crystalline states,[18] and a peak at low Q (around 1−2 nm^{-1}) referred to as the ionomer peak. The latter is the hydration-dependent fingerprint of hydrophobic/hydrophilic nanophase separation.[19] Its position, Q_{ion}, is extremely sensitive to water content and, thus, was frequently used as a precise signature of membrane swelling at the nanoscale.[20] Note that all data shown were taken at a fixed high relative humidity (85%) where the ionomer peak is intense and well-defined, with the purpose of unambiguously disentangling the eventual aging effects from any peak variations due to slightly different hydration conditions. An additional series of samples was also conditioned at 30%RH to check the lower hydration condition (see Supporting Information). In addition to the two well-defined maxima, the SAXS patterns also contain a significant small-angle upturn. This is due to the presence of a global arrangement of larger scale scattering objects associated with the presence of a low-angle peak at $Q \sim 0.2$ nm^{-1} (so-called matrix knee).[20,21]

The 2D patterns were radially averaged to obtain the 1D spectra $I(Q)$. y-Series of $I(Q)$ versus Q taken on both native and aged membranes are displayed in Figure 1b. The WAXS region is omitted because we found that aging has no detectable impact on the WAXS peak shape or intensity. The WAXS peak was found to be homogeneous over the (y,z) mesh and identical to that of the reference membrane. A two-component fit of the WAXS data indicates a value of ∼15% crystallinity. The set of data acquired on aged and native membranes are shown over the entire experimental Q-window in the Supporting Information (Figure S3). Long-term aging has no effect on the crystallinity of the perfluorinated nonreinforced backbone. This suggests that there is no significant chemical

dx.doi.org/10.1021/mz500179z | ACS Macro Lett. 2014, 3, 778−783

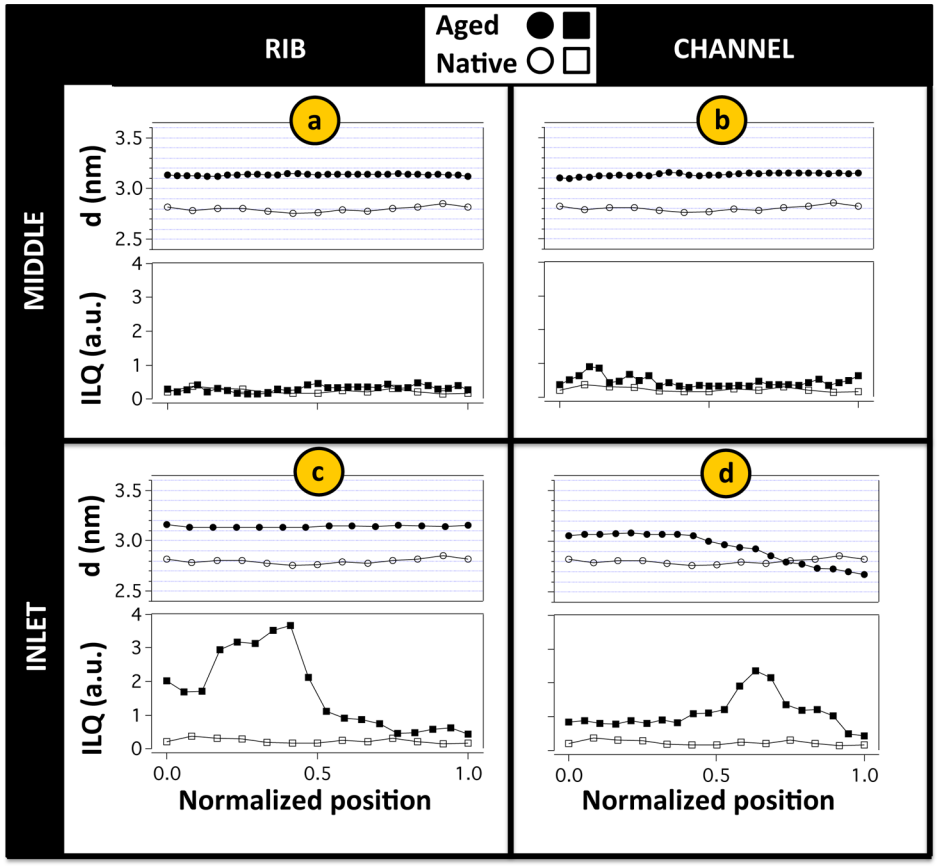

Figure 2. Measured values of d-spacing, $d = 2\pi/Q_{ion}$, and fitted values of the low angle scattering upturn, ILQ, as a function of the normalized y-scan position along membrane thickness (0 = anode side, 1 = cathode side) obtained for the native (hollow symbols) and for aged MEAs (solid symbols) at different fuel cell functional positions: (a) middle/rib (inset: same plot at detailed scale), (b) middle/channel, (c) inlet/rib, and (d) inlet/channel.

degradation of the polymer chains in relation with "soft" aging conditions. In contrast, significant effects are observed in the SAXS region (Figure 1b, example of the air inlet under the channel region sample). The spectra of the aged MEA vary considerably upon scanning along the membrane thickness. Three regions were colored in Figure 1b to selectively highlight the effects. Going from the anode side (A, blue) to the cathode side (C, green), one can first notice a clear change in the ionomer peak shape, position and intensity. The peak is shifted to higher Q-values, revealing that membrane swelling is reduced at the cathode. In the middle of the membrane thickness (red), the ionomer peak evolves into a poorly defined bump, and this is associated with a 10-fold increase of the small-angle upturn, as visualized by the dashed projection drawn on the 3D plot. Conversely, the microstructure of the native membrane is very homogeneous (Figure 1b): (i) the ionomer peak appears at a constant value of Q and has a uniform shape and intensity; (ii) no significant intensity variations of the small-angle upturn are detected.

Hence, direct examination of the raw μSAXS spectra y-series reveals that (i) aging modifies the membrane nanostructure, (ii) it has an impact on the microstructure at larger scales, and (iii) structural inhomogeneities are observed along the membrane thickness.

To get further insights into these effects, we performed a model-free empirical analysis of the 1D spectra (y,z) series to extract numerical values of the relevant parameters, that is, the ionomer peak position, Q_{ion}, and the low-angle scattering upturn in intensity, ILQ. A detailed description of the data analysis is provided in the Supporting Information (Figure S4). The variations of ILQ along membrane thickness, and from one sample to another, were evaluated by comparing the intensities values at a given low-Q value of 0.4 nm^{-1}. The ionomer peak position was determined using a phenomenological function accounting for background components and a Gaussian peak centered on Q_{ion}.

The d-spacing associated with the ionomer peak positions, $d = 2\pi/Q_{ion}$, characterizes the swelling of the polymer due to the adsorption of water.[22] This can be interpreted in two ways, depending on the model used to describe the PFSA membrane microstructure: mean separation distance between polymer ribbons packed in a locally semi-lamellar geometry[20,23] or water nanochannels hexagonally arranged in the polymer matrix.[21] Independently from the model, it is widely accepted that d-spacing values are highly dependent on the thermal history, preparation method, charge density, and hydration level.[24] Typically they range from 1 to 3 nm in PFSA membranes. The value in the native membrane is found equal to 2.8 nm at 85% RH and 2.6 nm at 30% RH.

The large heterogeneous membrane degradation is highlighted in Figure 2d and ILQ profiles of aged samples taken from the MEA close to air inlet or far from it (middle) are compared to those of the native membrane. Aged zones under the ribs or the channels were selected through z-scans to focus on the four functional positions of interest: middle/rib (a), middle/channel (b), inlet/rib (c), and inlet/channel (d). The variations of d and ILQ along membrane thickness are represented as a function of a normalized position, defined

dx.doi.org/10.1021/mz500179z | ACS Macro Lett. 2014, 3, 778−783

such that position 0 corresponds to the anode side and 1 to the cathode side. This normalized thickness is useful as small membrane misalignments were unavoidable, giving rise to apparent thicknesses variations with respect to the nominal 50 μm.

The native membrane displays a constant d-spacing and relatively constant value of ILQ across its thickness, with some low amplitude variations randomly distributed in the (y,z) plane. Conversely, we can assess from Figure 2 that aging has an unavoidable effect on the membrane morphology with an extent that depends on the operating position. In all aged positions, at least one of the parameters (d,ILQ) deviates from those of native membranes. The less affected profiles are those measured in the middle position, while the most pronounced effects are found in the inlet position.

A more detailed analysis of the d-spacing evolution evidence significant position-dependent effects. First, it is observed that the (a−c) profiles are remarkably flat. The absolute swelling is significantly higher compared to that of a native membrane: 3.20 nm in middle/ribs, 3.15 in inlet/ribs, and 3.10 in middle/channels, against the reference value of 2.80 nm. The appearance of a long-term evolving process originates from the continuous exposure to high temperatures in the presence of water during fuel cell operation, which deforms the microstructure of the membrane. The flat d-spacing profiles suggest that there are no significant variations of the water content across the membrane from the anode side to the cathode side during fuel cell operation. This effect is systematically observed (i) under the ribs, regardless of the relative position of the air inlet, and (ii) in the middle position. We tentatively assign this behavior to a combination of the operating conditions and the through-plane water distribution. This in turn is induced by the counter-flow configuration in the stack i.e. air inlet close to hydrogen outlet. In such a configuration both anode and cathode sides are fully humidified in the middle of the cell when current is supplied.[25] A constant water gradient concentration is thus maintained far from the air manifolds. As well as the effects of the counter-flow configuration, it has been demonstrated that water usually accumulates under the ribs everywhere in the active surface area during fuel cell operation.[26] A homogeneous hydration is thus expected to be found under the ribs regardless of the inlet or middle position.[27] This is consistent with the μSAXS analysis of Figure 2a−c. In contrast, the situation appears to be strikingly different in the (d) position, that is, close to air inlet under the channels, where a clear anode/cathode inhomogeneity is detected. As the ionomer peak position is continuously shifted to higher Q vectors (Figure 1b), we obtain a highly dispersed profile with swelling to 3.1 nm at the anode, and shrinking to 2.6 nm at the cathode, compared to the uniform profile of 2.8 nm observed for the native membrane. Such dispersion in terms of the swelling property of the aged membrane certainly indicates the existence of a highly inhomogeneous water distribution across membrane thickness in the inlet/channel region. Our results unambiguously indicate the presence of a strong gradient of water concentration from anode to cathode, with an excess of water at the anode. The counter-flow configuration induces water saturation at the anode outlet whereas on the opposite side, that is, air inlet, the membrane is in contact with a gas close to 75% relative humidity. The dispersed (d) profile provides direct evidence of these peculiar operating conditions and their consequences on long-term swelling properties of the aged membrane.

Further inspection of the low-angle intensity variations points out some additional differences between the structural changes occurring in the rib and channel regions. Far from gas inlet, the ILQ profiles across thickness are rather flat, with values slightly higher to the native membranes and more scattered, especially in the channel (see the inset of Figure 2a,b). Close to the air inlet, however (Figure 2c,d), the absolute ILQ values are much more pronounced than the random variations observed for the native membrane, as was already clear from the projections of Figure 1b. The low-Q intensities, ILQ, show considerable variation reaching a maximum value almost 1 order of magnitude higher when compared to the anode/cathode extremities. These findings suggest that aging provokes the development of microstructural heterogeneities at a scale of 20−50 nm. It can be hypothesized that the low angle effects may arise from large scale polymer matrix reorganization under the prolonged mechanical constraints. Such constraints are particularly severe near the air inlet, where the most significant ILQ features are found (Figure 2c,d), due to important water concentration profiles across the membrane thickness established in this region.[28] An alternative hypothesis regarding the low-Q effects may come from the presence of platinum nanoparticles issued from electrode degradation.[9] However, SEM images taken on the degraded membrane revealed that Pt nanoparticles are found at a very low concentration (less than 0.1% in volume, see Figure S1), which is unlikely to produce the spectacular low-angle accidents. The Pt nanoparticles are preferentially distributed close to the cathode and show a homogeneous in-plane repartition inside the bulk material. No evidence of the formation of a thin dense Pt layer was found, as would be expected in the case of aggressive open circuit voltage tests leading to intense electrode/membrane chemical degradations.[1,29] The low-Q effects concentrate at the cathode side under the channels, but they are even more intense at the anode side under the ribs. This could arise from the local stress, along with anode/cathode water repartition, which might differ in front of the rib and in front of the channel.[30,31]

In-plane and through-plane heterogeneities were evidenced by μSAXS for a MEA aged 2500 h in a stack in counter-flow configuration under stationary conditions. On the basis of the quantitative analysis of the 3D scattering mappings recorded on aged regions, as compared to the native membrane, we can evidence two major physical degradation mechanisms having a different impact on the microstructure of the various zones under investigation: expansion at the level of the ionic domains (modification of the nanoscopic membrane swelling) and higher scale heterogeneities (typically 20−50 nm).

(i) The degradation is not homogeneous and is highly dependent on the local operating conditions, that is, on the positions relative to anode/cathode, ribs/channels and inlet/middle. Regions under ribs and channels far from air inlet undergo smallest aging effects. Regions close to the air inlet experience more severe deterioration. The zones under channels in the vicinity of the air inlet are subjected to major microstructural modifications, both in terms of swelling and large-scale polymer organization. We can rationalize these findings on the basis of the heterogeneous distribution of water in the counter-flow condition of the PEMFC stack. When current is produced, the membrane sorbs water. The water gradient concentration from cathode to anode is

dx.doi.org/10.1021/mz500179z | ACS Macro Lett. 2014, 3, 778−783

larger close to the air inlet and the internal stress induced by the swelling is likely to provoke a serious degradation in this part of the cell.

(ii) Prolonged exposure of the membrane to hot water induces an "irreversible" modification of the membrane swelling that could reflect a continuous polymer matrix deformation due to backbone relaxations, as previously observed in ex situ swelling kinetics studies.[32,33] After 2500 h in a stack, the *d*-spacing is increased by 3−4 Å in some regions of the aged membrane with respect to a native one, such that additional water molecules can be further accommodated in the network of much expanded interconnected ionic domains. This overswelling effect is always observed in front of the ribs, probably because the gas diffusion layers remain full of stagnant water during operation.[26] In front of the channels, it depends on the position in the cell. In other words, the drying effect close to the air inlet restrains the long-term effect especially on the cathode side (Figure 2d).

(iii) The aging of a membrane in an operating PEMFC stack produces physical heterogeneities that develop over an extended range of length scales, starting from nanoscale phenomena (ionic domains swelling, polymer reorganization) up to the centimeter scale, that is, the overall size of the fuel cell active area. Anode/cathode variations and effects along the membrane thickness are found at a micrometer scale, while in-plane differences in front of the ribs and the channels occur at a millimeter scale. Only by sampling an aged MEA in-plane and along its thickness with a microfocused X-ray beam allowing submicrometer resolution can we simultaneously cover all the characteristic distances of interest for a multiscale investigation.

In conclusion, we have shown that the μSAXS technique is an extremely valuable tool for unveiling the physical degradation processes in polymer electrolytes, as we can directly correlate the scattering profiles in terms of shape and intensities to the microstructural state of the membrane inside an aged MEA. This is a convenient method providing meaningful data to assess the nature, the localization, and the severity of the degradation effects. In the rather soft aging conditions of the present stack test, no substantial chemical degradation was induced. No H_2 crossover was measured during 2500 h, the amount of pollutants arising from electrode degradation is low, and we found no modifications in polymer crystallinity. Hence, μSAXS experiments give a unique insight into important physical aging phenomena prior to any massive chemical degradation. It could be employed on a variety of other MEAs integrated in specific fuel cell designs operated in a range of interesting conditions. Overall, this work provides a framework for comprehensive diagnostics with implications toward building strategies to design more durable polymers inserted in smart fuel cell designs. It opens the path to forthcoming degradation studies of a panoply of solid electrolytes including advanced materials as electrodes for Li-ion batteries.

■ ASSOCIATED CONTENT

Supporting Information

More details about the samples, the experimental setup, the data acquisition, and reduction and analysis. This material is available free of charge via the Internet at http://pubs.acs.org.

■ AUTHOR INFORMATION

Corresponding Author

*E-mail: arnaud.morin@cea.fr.

Present Address

†Laboratoire TIMC-IMAG, 38706 La Tronche cedex, France (M.M.).

Notes

The authors declare no competing financial interest.

■ ACKNOWLEDGMENTS

M.M. has been funded by the New Technologies for Energy CEA cross-division program in the framework of DIGEST project. We acknowledge the European Synchrotron Radiation Facility (ESRF) for allocation of beam time, Dr. M. Sztucki for technical support during the experiment, and C. Montero for setting up the humidity control environment. Laure Guétaz is acknowledged for taking the SEM images.

■ REFERENCES

(1) Borup, R. L.; et al. *Chem. Rev.* **2007**, *107*, 3904−3951.
(2) Subianto, S.; Pica, M.; Casciola, M.; Cojocaru, P.; Merlo, L.; Hards, G.; Jones, D. J. *J. Power Sources* **2013**, *233*, 216−230.
(3) Rodgers, M. P.; Bonville, L. J.; Kunz, R. K.; Slattery, D. K.; Fenton, J. M. *Chem. Rev.* **2012**, *112*, 6075−6103.
(4) Dubau, L.; Durst, J.; Maillard, F.; Chatenet, M.; André, J.; Rossinot, E. *Fuel Cells* **2012**, 188−198.
(5) Li, Y.; Dillard, D. A.; Case, S. W.; Ellis, M. W.; Lai, Y. H.; Gittleman, C. S.; Miller, D. P. *J. Power Sources* **2009**, *194* (2009), 873−879.
(6) Aindow, T. T.; O'Neill, J. *J. Power Sources* **2011**, *196*, 3851−3854.
(7) Kreitmeier, S.; Schuler, G. A.; Wokaun, A.; Büchi, F. N. *J. Power Sources* **2012**, *212*, 139−147.
(8) Yan, Q. G.; Toghiani, H.; Lee, Y. W.; Liang, K. W.; Causey, H. *J. Power Sources* **2006**, *160*, 1242−1250.
(9) Guétaz, L.; Escribano, S.; Sicardy, O. *J. Power Sources* **2012**, *212*, 169−178.
(10) Collier, A.; Wang, H.; Yuan, X. Z.; Zhang, J.; Wilkinson, D. P. *Int. J. Hydrogen Energy* **2006**, *31*, 1838−1854.
(11) Kundu, S.; Karan, K.; Fowler, M.; Simon, L. C.; Peppley, B.; Halliop, E. *J. Power Sources* **2008**, *179*, 693−699.
(12) Danilczuk, M.; Lancucki, L.; Schlick, S.; Hamrock, S. J. *ACS Macro Lett.* **2012**, *1*, 280−285.
(13) Gebel, G.; Diat, O. *Fuel Cells* **2005**, *5*, 261−276.
(14) Blachot, J. F.; Diat, O.; Putaux, J.-L.; Rollet, A.-L.; Rubatat, L.; Vallois, C.; Müller, M.; Gebel, G. *J. Membr. Sci.* **2003**, *214*, 31−42.
(15) Mendil- Jakani, H.; Davies, R. J.; Dubard, E.; Guillermo, A.; Gebel, G. *J. Membr. Sci.* **2011**, *369*, 148−154.
(16) Pineri, M.; Gebel, G.; Davies, R. J.; Diat, O. *J. Power Sources* **2007**, *172*, 587−596.
(17) Developed at the CNRS *Laboratoire de Physique des Solides*, Paris, France; http://www.lps.u-psud.fr/.
(18) Mauritz, K. A.; Moore, R. B. *Chem. Rev.* **2004**, *104*, 4535−4585.
(19) Gierke, T. D.; Munn, G. E.; Wilson, F. C. *J. Polym. Sci.* **1981**, *19*, 1687−1704.
(20) Rubatat, L.; Rollet, A.-L.; Gebel, G.; Diat, O. *Macromolecules* **2002**, *35*, 4050−4055.
(21) Schmidt-Rohr, K.; Chen, Q. *Nat. Mater.* **2008**, *7*, 75−83.
(22) Kusoglu, A.; Modestino, M. A.; Hexemer, A.; Segalman, R. A.; Weber, A. Z. *ACS Macro Lett.* **2012**, *1*, 33−36.
(23) Kreuer, K.-D.; Portale, G. *Adv. Funct. Mater.* **2013**, *23*, 5390−5397.
(24) Liu, Y.; et al. *Macromolecules* **2012**, *45*, 7495−7503.
(25) Mishler, J.; Wang, Y.; Mukundan, R.; Spendelow, J.; Hussey, D. S.; Jacobson, D. L.; Borup, R. L. *Electrochim. Acta* **2012**, *75*, 1−10.
(26) Fairweather, J. D.; et al. *J. Electrochem. Soc.* **2013**, *160*, F980−F993.

(27) Deevanhxay, P.; Sasabe, T.; Tsushima, S.; Hirai, S. *Int. J. Hydrogen Energy* **2011**, *36*, 10901−10907.
(28) Xu, F.; Diat, O.; Gebel, G.; Morin, A. *J. Electrochem. Soc.* **2007**, *154*, B1389−B1398.
(29) Ferreira, P. J.; La O', G. J.; Shao-Horn, Y.; Morgan, D.; Makharia, R.; Kocha, S.; Gasteiger, H. A. *J. Electrochem. Soc.* **2005**, *152*, A2256−A2271.
(30) Boillat, P.; et al. *Electrochem. Commun.* **2008**, *10*, 546−550.
(31) Kusolglu, A.; Karlsson, A. M.; Santare, M. H.; Cleghorn, S.; Johnson, W. B. *J. Power Sources* **2007**, *170*, 345−358.
(32) Sutor, A. K.; Huguet, P.; Morin, A.; Gebel, G.; Le, T. S.; Deabate, S. *Fuel Cells* **2012**, *12*, 162−168.
(33) Alberti, G.; Narducci, R.; Sganappa, M. *J. Power Sources* **2008**, *178*, 575−583.